Environmental Science & Technology

Article

Cite This: Environ. Sci. Technol. XXXX, XXX, XXX−XXX

pubs.acs.org/est

Oxidative Potential of Water-Soluble Matter Associated with Chromophoric Substances in $PM_{2.5}$ over Xi'an, China

Qingcai Chen,*[,†] Mamin Wang,[†] Yuqin Wang,[†,‡] Lixin Zhang,[†] Yanguang Li,[§,∥] and Yuemei Han[⊥]

[†]School of Environmental Science and Engineering, Shaanxi University of Science and Technology, Xi'an 710021, China

[‡]Department of Earth and Atmospheric Sciences, Saint Louis University, St. Louis, Missouri 63108, United States

[§]Key Laboratory for the Study of Focused Magmatism and Giant Ore Deposits, MLR, Xi'an 710054, China

[∥]Xi'an Center of Geological Survey, China Geological Survey, Xi'an 710054, China

[⊥]Key Laboratory of Aerosol Chemistry and Physics, State Key Laboratory of Loess and Quaternary Geology, Institute of Earth Environment, Chinese Academy of Sciences, Xi'an 710061, China

Supporting Information

ABSTRACT: Organic compounds are important contributors to the oxidative potential (OP) of atmospheric aerosols. This study is the first to report the OP of water-soluble organic matter (WSOM) related to the chromophoric substances in $PM_{2.5}$ over Xi'an, China. The dithiothreitol (DTT) activity levels in $PM_{2.5}$ extracted by water were quantified as well as the relationships between DTT activity and light absorption and fluorescence properties. The results show that the DTT activity has significantly correlated with colored WSOM, in which we identified three light absorbing substances (BrC1−3) and eight fluorescent substances (C1−8). It is further found that BrC3 and C7 accounted for almost all of the DTT activity by colored WSOM, although these two factors contributed only a small fraction of light absorption and fluorescence. BrC3 and C7 are clearly distinguished from other chromophoric substances because of their long absorption wavelength (λ_{max} = 475 nm) and fluorescence emission wavelength (λ_{max} = 462 nm), respectively. This discovery will help to better interpret and understand the mechanism of oxidation activity generation by light absorbing organic aerosols and provide guidance for predicting the OPs of light absorbing organic aerosols based on their optical properties.

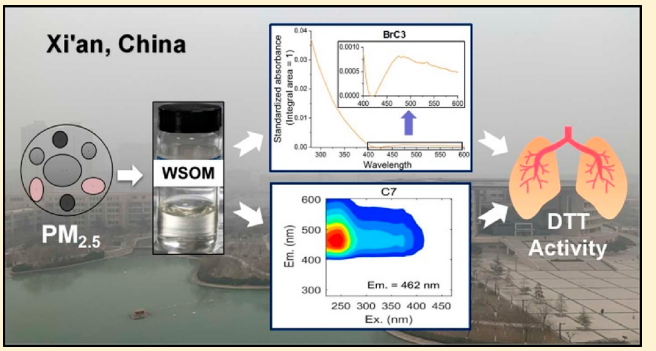

INTRODUCTION

A large number of epidemiological studies have shown that atmospheric particulate matter (PM) can harm human health.[1−3] The generally accepted toxicological mechanism is the oxidative stress effect of the body by reactive oxygen species (ROS), also known as redox activity or excessive accumulation of oxidative potential (OP).[4,5] There are three main ways in which PM induces ROS in the body: (1) oxidants in the particles are deposited in the respiratory system; (2) certain chemical components in the particles stimulate the cells to produce excess ROS; and (3) certain chemical components in the particles catalyze the interaction with specific biochemicals that produce ROS.[4,6,7] PM chemical components can interact with airway epithelial cells and macrophages to produce ROS,[8] which can cause damage to cells.[6,9,10] This damage is associated with respiratory inflammation, cardiovascular effects, and other adverse health effects.[11−14]

The dithiothreitol (DTT) assay is a widely used noncellular method for determining oxidation activity[15] by mimicking the oxidative levels of cellular reducing agents, such as NADPH, and it can be used to assess the OP of atmospheric PM by the rate of DTT consumption.[13] The current DTT assay focuses on the OP of the water-soluble matter (WSM) in PM and explores the intrinsic link between the chemical composition of PM and the DTT consumption rate. Studies have shown that components such as quinones,[15] humic-like substances (HULIS),[16−18] and transition metals[19,20] in PM have DTT activity. Among them, studies have found that Cu and Mn are the water-soluble transition metals with the highest DTT activity contributions.[21]

Studies have shown that water-soluble organic matter (WSOM) is closely related to DTT activity.[16,22] Lin and Yu[16] found that HULIS account for 79% of the DTT activity of the WSM in PM and believe that HULIS are a major contributor to DTT activity. Verma et al.[22] found that the DTT activity of the WSM in PM has a significant positive

Received: April 2, 2019
Revised: June 25, 2019
Accepted: June 28, 2019
Published: June 28, 2019

DOI: 10.1021/acs.est.9b01976
Environ. Sci. Technol. XXXX, XXX, XXX−XXX

correlation with brown carbon (BrC) but is not correlated with any metals. These studies indicate that organic matter has an important contribution to the DTT activity of PM and may be mainly BrC species. However, to the best of our knowledge, the intrinsic relationship between BrC and OP has not been thoroughly explored from the viewpoint of the optical properties of PM. Some of the substances in BrC can produce a fluorescent signal, and the chromophore can provide more information about organic species. However, the chromophore substances that have DTT activity or the mechanism by which chromophore substances produce DTT activity have not been elucidated. To this end, this study investigated in depth the DTT consumption associated with colored WSOM in PM and explored the intrinsic link between the optical properties and DTT consumption levels.

This study analyzed the DTT activity of the WSM in $PM_{2.5}$ in the spring, summer, autumn, and winter of 2017 over Xi'an as well as the absorbance characteristics (ultraviolet−visible (UV−Vis) spectrum) and fluorescence characteristics (excitation−emission matrix (EEM) spectrum) of the WSM in the $PM_{2.5}$. The UV−Vis spectral and EEM spectral data coupled with the DTT activities were analyzed by a factor analysis method, and the relative contributions of different types of chromophoric substances to the DTT activity were obtained. The mechanism of DTT activity by chromophoric substances was also discussed. The results of this study will help to increase our understanding of the mechanism of OP generation by atmospheric aerosols.

MATERIALS AND METHODS

Sample Collection. $PM_{2.5}$ sample collection was performed with a high-volume sampler equipped with a $PM_{2.5}$ cutting head (XT-1025, Shanghai Xintuo, China). The sampling position was set at the top of Shaw House, Shaanxi University of Science and Technology, Xi'an, China (34° 22′ 35.07″ N and 108° 58′ 34.58″ E at 420 m above sea level or 40 m above ground level). A total of 112 samples were collected in 2017 (details in Tables S1−S4 of the Supporting Information). The sampling start time was 7:00 local time (Beijing time), the sampling duration was 23.5 h, and the air flow rate was 1000 L/min. The $PM_{2.5}$ samples were collected on a 20 × 25 cm prefired quartz glass fiber filter in an aluminum foil bag and stored in a refrigerator at −20 °C.

Sample Extraction. WSM extraction was used for the DTT assay as well as water-soluble organic carbon (WSOC), light absorption, and EEM analysis. The sample for the DTT assay was obtained by extracting a 5 mm diameter filter punch using 2 mL of ultrapure water by vortex mixing (Model MX-S, SCILOGEX, USA) for 5 min and then filtering with a polytetrafluoroethylene (PTFE) filter (0.45 μm, JINTENG, China). The sample used to analyze the WSOC was obtained by using a filter punch of 8 mm in diameter and then ultrasonically extracted with 20 mL of ultrapure water for 30 min before filtering with a 0.45 μm PTFE filter. The samples used for the optical property analysis were obtained by using a 9 mm diameter filter punch and then ultrasonically extracted with 6 mL of ultrapure water for 30 min before filtering with a 0.45 μm PTFE filter. To avoid the sample being affected by a concentration difference during the analysis, the sample dilution factor was adjusted to obtain a concentration within the same order of magnitude before the measurement. A blank analysis and parallel sample analysis were performed for all analytical methods. The blank and parallel samples were analyzed for blank calibration and to verify the extraction process and reproducibility of analytical results.

Chemical Composition Analysis. WSOC analysis was performed using a total organic carbon (TOC) analyzer (Sievers M9, General Electric, USA). We used the off-line analysis mode to measure the same sample three times and calculated the average. To ensure the data quality of the sample, our analysis was performed within 30 min of sample extraction. At the same time, we set background measurements for each batch of experiments to deduct background interference. At the same time, the final WSOC concentration was adjusted to 0.1−1 ppm by adjusting the sample dilution factors for the different concentrations of the sample. The standard curve was based on the analysis of a range of different concentrations (0−1 ppm) of glucose standard solutions, and it was used for data correction.

Other chemical analyses included elemental carbon (EC), water-soluble ion, and elemental analyses, which are detailed in the Supporting Information. Briefly, an EC analysis was conducted using a thermo-optical carbon analyzer (DRI Model 2001A) with an IMPROVE_A heating protocol. A water-soluble ion analysis was performed by ion chromatography (940 Professional IC Vario, Metrohm, Switzerland). The elemental analysis is based on the analytical method by Chen et al.[23] using laser ablation (LA, GeoLas Pro, Coherent, Germany) combined with inductively coupled plasma mass spectrometry (ICP-MS, 7700x, Agilent, USA). The elemental analysis detects all forms of elemental concentrations in $PM_{2.5}$ samples, including water-soluble and water-insoluble elements.

UV−Vis Absorption Spectra and EEM Fluorescence Spectra. The extract was transferred to a quartz cuvette with a path length of 1 cm, and the UV−Vis absorption spectra and EEM fluorescence spectra were obtained with an AquaLog fluorometer (HORIBA, Japan). The UV−Vis absorption spectra were recorded in the range of 200−600 nm with a wavelength interval of 5 nm. Ultrapure water was also analyzed for baseline correction prior to scanning a series of extracts. The excitation wavelengths of the EEMs were measured in the range of 200−600 nm. The emission wavelengths were in the range of 250−600 nm. The scanning speed was 600 nm min^{-1}, the scanning interval was 5 nm, and the exposure time was 0.5 s. The WSOC concentrations of all samples were controlled within 10 ppm so that all samples had an absorbance of less than 0.5 at 250 nm to reduce the effect of the internal rate effect, which is a phenomenon in which the fluorescence is weakened due to the absorption of the excitation light or the emitted light by the fluorescent substance or other light absorbing substance when the concentration of the fluorescent substance is large or coexists with other light absorbing materials.

The UV−Vis absorption spectra were processed minus the background sample interference. The EEM data were calibrated as described by Lawaetz and Stedmon[24] and Murphy et al.,[25] including instrument calibration, internal filter correction, Raman and scattering removal, data smoothing, and background interference subtraction.[24]

OP Analysis. The DTT assay is a commonly used noncellular method for quantifying PM OP. In the DTT analysis, DTT is consumed by the active oxygen and oxidized to produce disulfides. Therefore, the oxidation activity of PM is quantitatively evaluated by the consumption rate of DTT. The determination of the DTT activity in this study was based on the method proposed by Cho et al.[13] First, 0.5 mL of a DTT

DOI: 10.1021/acs.est.9b01976
Environ. Sci. Technol. XXXX, XXX, XXX−XXX

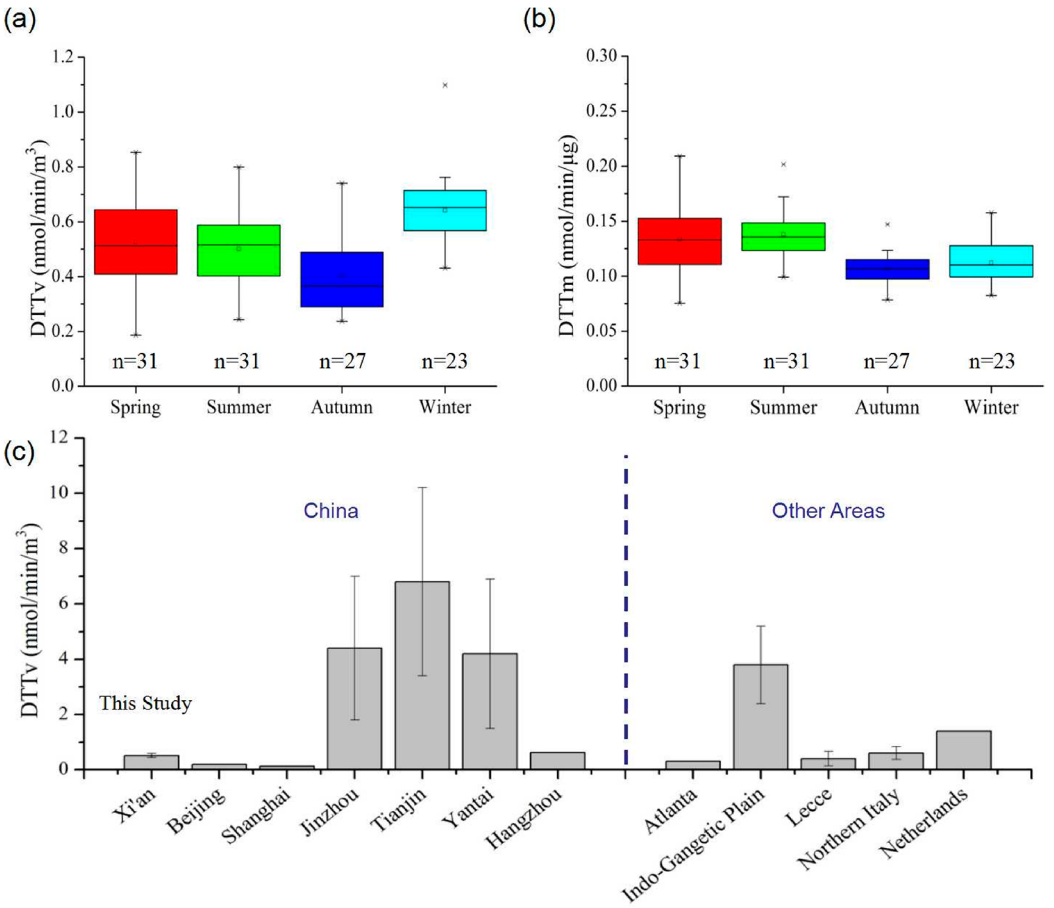

Figure 1. DTT consumption rates of the water-soluble substances in $PM_{2.5}$ over Xi'an in the spring, summer, autumn, and winter seasons of 2017. (a) DTTv consumption rate per unit atmospheric volume. (b) DTTm consumption rate per unit WSOC. (c) DTT consumption rates for Xi'an, Beijing,[33] Shanghai,[34] Jinzhou,[27] Tianjin,[27] Yantai,[27] Hangzhou,[36] Atlanta,[18] Indo-Gangetic Plain,[37] Lecce,[35] the Northern Italian Alpine Region,[38] and The Netherlands.[39] The error bars in the figure represent the standard deviation.

solution (1 mM, ≥ 98%, Sigma-Aldrich, prepared with a phosphate buffer at pH = 7.4) was mixed with 0.5 mL of the sample filtrate, and the sample was reacted in a 37 °C water bath. The sample reaction was carried out at 0, 4, 13, 23, 32, and 41 min. Then, the reaction was terminated by adding 0.1 mL of the above mixture to a centrifuge tube containing 1 mL of trichloroacetic acid (1%, w/v). Then, 0.5 mL of 5,5′-dithiobis(2-nitrobenzoic acid) (DTNB, 0.2 mM, ≥ 98%, Sigma-Aldrich) and 2 mL of Tris buffer (0.08 M with 4 mM EDTA) were added to the mixture for color development. Finally, the absorbance of the sample at 412 nm (Abs_{412}) was measured by a UV−Visible absorption spectrometer (Aqua-Log, HORIBA, Japan). The concentration of DTT in the sample solution was quantitatively analyzed by the value of Abs_{412}, and the consumption rate of DTT (unit: μM/min) was calculated based on the remaining DTT concentration in the sample at different reaction times. In this experiment, the concentration of DTT varies linearly with time and is a zero-order kinetic reaction, which is the same as reported in other studies.[13] This fact indicates that the active oxygen-generating substance in the PM mainly acts as a catalyst and is itself not consumed. This result also means that the DTT consumption may not be mainly caused by the organic hydroperoxides.[26]

The PM concentrations in different seasons are different (range: 15−179 $\mu g/m^3$, Table S1−S4). It has been reported that the correlation between DTT consumption rate and PM concentration is not high.[27,28] Therefore, to reduce the possible influence of the difference in sample concentrations on the DTT analysis results, the WSOC concentration of the sample at the time of detection was controlled in the range of 1−10 ppm. To reduce possible interference during the experiment, the whole experimental process was carried out as much as possible in the dark while ensuring that all samples were tested within 2 h. In addition, blank sample analysis and parallel sample analysis were also performed for background correction and to verify the reproducibility of the analysis results. As shown in Figure S1, the background sample consumption rate is 0.045 ± 0.004 μM/min, indicating that the background sample has some interference, although the effect on the actual sample is limited, and the background value contributes an average of 18 ± 5% to all of the samples. The average DTT consumption rate of ultrapure water was 0.030 ± 0.003 μM/min. A comparison with the results of the background samples shows that the main interference is not from the background sample but from the ultrapure water or the analytical process, which may be the self-oxidation of DTT leading to the consumption of DTT in ultrapure water. Nonetheless, the final background effect was deducted in this study. The reproducibility of the entire analysis was determined by separately extracting and analyzing the DTT activity of the same sample, and the results showed that the relative standard deviation of the DTT consumption rate analysis result was 4%.

DOI: 10.1021/acs.est.9b01976
Environ. Sci. Technol. XXXX, XXX, XXX−XXX

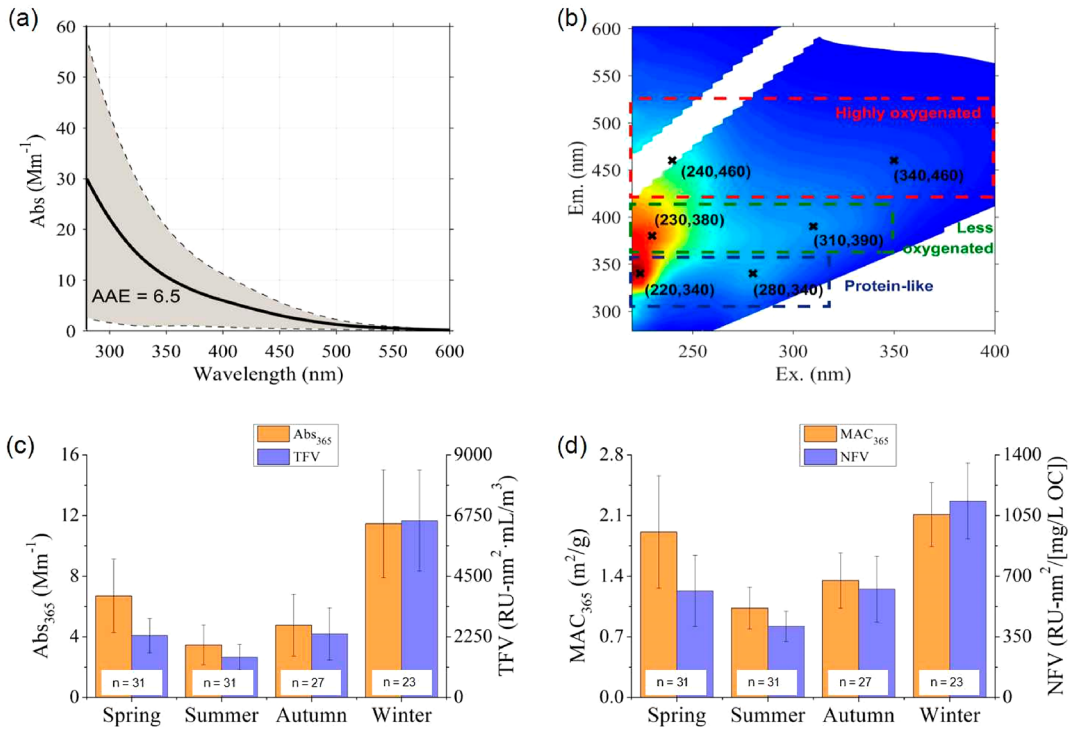

Figure 2. Annual average absorption spectra (a) and EEM spectra (b) of the water-soluble substances in the $PM_{2.5}$ samples. (c) Four season absorbance (Abs_{365}, Mm^{-1}) and TFV ($RU\text{-}nm^2\cdot mL/m^3$). (d) Mass absorption coefficient (MAC_{365}, m^2/g) and FV by the WSOC concentration (NFV, $RU\text{-}nm^2/[mg/L\ OC]$). (a) Shaded area in the figure represents the standard deviation, and the error bars in (c) and (d) represent the standard deviations of Abs_{365} and TFV for the four season samples, respectively.

Factor Analysis of the DTT Data Coupled with the UV−Vis Absorption and EEM Spectra. To evaluate the relative contributions of the different types of chromophoric substances to the DTT activity, this study used factor analysis methods. A parallel factor analysis (PARAFAC) and non-negative matrix factorization (NMF) resolved the DTT activity data coupled with the UV−Vis absorption and EEM spectra, respectively. NMF has been widely used in spectral analysis.[29] The coupling of the DTT data with the EEM and absorption spectrum data sets and applying factor analysis are innovations in this study, which evaluate the relative contributions of different factors to the DTT activity. The basic principles of PARAFAC and NMF in this study are as follows:

$$X_{n,i,j} = \sum_{f=1}^{F} a_{n,f}\cdot(b_{i,f}c_{j,f}) + e_{n,i,j} \quad (1)$$

$$Y_{n,k} = \sum_{f=1}^{F} a_{n,f}\cdot g_{f,k} + e_{n,k} \quad (2)$$

where n is the number of samples 1, ..., N; i = 1, ..., I; j = 1, ..., J; k = 1, ..., K; $X_{n,i,j}$ represents the DTT data ($X_{n,I,J}$) coupled with the EEMs ($X_{n,1...I-1,1...J-1}$); $Y_{n,k}$ represents the DTT data ($X_{n,K}$) coupled with the light absorption spectra ($Y_{n,1...K-1}$); f is the number of factors; a is the load factor; b, c, and g contain factor spectrum information; and $e_{n,i,j}$ represents the model residuals.

The DTT data coupled with the EEMs were analyzed using the drEEM toolkit (http://www.models.life.ku.dk/dreem) in MATLAB version 0.2.0.[30] The detailed model analysis procedure is based on previous studies by Chen et al.[31] According to the component EEM characteristics of the 2−15 component PARAFAC model and the residual error trend of the model (Figure S2), the 8 component PARAFAC model was selected.

The NMF analysis was performed on the DTT data coupled with the UV−Vis absorption spectra using the NMF Toolbox version 1.4 (https://sites.google.com/site/nmftool/) in MATLAB.[32] The detailed model analysis procedure is based on previous studies by Chen et al.[31] First, a solution is found from a plurality of random starting values using a gradient descent-based multiplication algorithm, and then the final solution is found from the first solution using a least-squares effective set algorithm. To find a global solution, the model was run 100 times, each time with a different initial value. By comparing the residuals of the 1−5 factor model (Figure S3) and the spectral load, a 3-factor NMF model was finally selected.

RESULTS AND DISCUSSION

DTT Activity of the Sample. Figure 1 shows the DTT activity levels and seasonal variation in the $PM_{2.5}$ samples from the spring, summer, autumn, and winter over Xi'an in 2017. Figure 1a shows the DTT activity in the atmospheric volume (DTTv, $nmol/min/m^3$), and the average levels from high to low are winter > spring > summer > autumn: winter: 0.64 $nmol/min/m^3$ (range: 0.43−1.10 $nmol/min/m^3$); spring: 0.53 $nmol/min/m^3$ (range: 0.19−0.85 $nmol/min/m^3$); summer: 0.50 $nmol/min/m^3$ (range: 0.24−0.80 $nmol/min/m^3$); and autumn: 0.40 $nmol/min/m^3$ (range: 0.24−0.74 $nmol/min/m^3$). The t test results show that the variation of DTTv consumption rate in each season is not distinct (p > 0.05). Figure 1c shows a comparison of the DTT activity of the PM over Xi'an with those over other regions in the study. The average DTTv activity over Xi'an in 2017 is 0.51 $nmol/min/m^3$, which is higher than those over Beijing (0.19 $nmol/min/$

DOI: 10.1021/acs.est.9b01976
Environ. Sci. Technol. XXXX, XXX, XXX−XXX

m^3)[33] and Shanghai (0.13 nmol/min/m^3)[34] in China, Atlanta in the United States (0.31 nmol/min/m^3),[18] and Lecce in southern Italy (0.40 ± 0.26 nmol/min/m^3)[35] but lower than those over the coastal cities of the Bohai Sea, northern China (Jinzhou: 4.4 ± 2.6 nmol/min/m^3; Tianjin: 6.8 ± 3.4 nmol/min/m^3; and Yantai: 4.2 ± 2.7 nmol/min/m^3),[27] Hangzhou, China (0.62 nmol/min/m^3),[36] the Indo-Gangetic Plain (3.8 ± 1.4 nmol/min/m^3),[37] the alpine region of northern Italy (0.60 ± 0.23 nmol/min/m^3),[38] and The Netherlands (1.4 nmol/min/m^3).[39]

Figure 1b shows the DTT activity per unit of WSOC (DTTm), with an average DTTm of 0.12 nmol/min/μg for 2017. The average DTTm values vary from season to season, from high to low for summer > spring > winter ≈ autumn: summer: 0.14 nmol/min/μg (range: 0.10−0.20 nmol/min/μg); spring: 0.13 nmol/min/μg (range: 0.08−0.21 nmol/min/μg); winter: 0.11 nmol/min/μg (range: 0.08−0.16 nmol/min/μg); and autumn: 0.11 nmol/min/μg (range: 0.08−0.15 nmol/min/μg). The t test results show that the variation of DTTm consumption rate in each season is not distinct ($p > 0.05$). Figures 1a and 1b show that the DTTv consumption rate in winter is higher than that in the other seasons while the DTTm consumption rate in winter is lower than that in the other seasons. This result indicates that although the PM and WSOC concentrations are high in winter (Table S4), the DTT consumption rates of the PM and WSOC are relatively low. In contrast, the PM and WSOC have the most DTT activity in summer, which should be related to its chemical composition and source.[27] For example, the strong photochemical reactions in summer can produce secondary organic aerosols containing naphthalene SOA, while quinone and semiquinone in naphthalene SOA react with oxygen to generate free radicals.[40]

Optical Characteristics of the Sample. We study the optical properties of the water-soluble PM to understand the mechanism by which water-soluble PM produces ROS. Figure 2 reflects the light absorption and fluorescence properties of the $PM_{2.5}$ sample over Xi'an, and Figures 2a and 2b show the average absorption (Abs) and EEM spectra of all samples, respectively. The absorption spectrum has no notable absorption peak, and its absorbance rapidly decreases as the wavelength increases. The wavelength dependence index AAE is 6.5, which is similar to those of the low-polarity HULIS of Japan's Nagoya researched by Chen et al.,[41] the WSM in the Los Angeles PM by Zhang et al.,[42] and the Beijing biomass burning PM by Yan et al.[43] Huang et al.[44] studied $PM_{2.5}$ samples from Xi'an in the summer of 2008 to the summer of 2009. The researchers reported that the absorption AAE values of the water-soluble BrC are similar to those in this study.

The EEM spectrum shows that the main fluorescent signal is present in the proteinlike and less oxygenated chromophore regions, with the strongest peaks appearing at approximately Peak (Ex. = 220 nm, Em. = 340 nm) and Peak (230 nm, 380 nm), respectively. However, studies have revealed that the proteinlike chromophore is most likely composed of phenolic compounds rather than amino acids.[31] In addition, several other peaks are shown in the EEM diagram, including Peak (240 nm, 460 nm), Peak (280 nm, 340 nm), and Peak (310 nm, 390 nm). The above EEM characteristics did not change significantly for the different seasonal samples over Xi'an, indicating that the main chromophore type and relative content did not change significantly with seasonal changes.

Figure 2c shows the seasonal variation in the absorbance (Abs_{365}, absorbance at 365 nm) and total fluorescence volume (TFV, RU-nm^2·mL/m^3). The Abs_{365} values of the spring, summer, autumn, and winter are 6.70 ± 2.4, 3.47 ± 1.3, 4.76 ± 2.0, and 11.46 ± 3.6 Mm^{-1}, respectively, which are higher than those of Los Angeles and Atlanta[45] and lower than that of Beijing.[46] Figure 2d shows the seasonal variations in the mass absorption coefficient (MAC_{365}, Abs_{365}·ln(10)/WSOC, m^2/g) and the FV normalized by the WSOC concentration (NFV, RU-nm^2/[mg/L OC]), which are basically consistent with the seasonal variations in Abs_{365} and TFV. The MAC_{365} values of spring, summer, autumn, and winter are 1.91 ± 0.65, 1.03 ± 0.24, 1.35 ± 0.32, and 2.11 ± 0.37 m^2/g, respectively. The MAC_{365} value of this study is higher than the values found in the Los Angeles basin and aerosols transmitted from northern China.[42,47] Huang et al.[44] studied atmospheric aerosol samples from Xi'an in the summer of 2008 to the summer of 2009. The Abs_{365} value studied by Huang et al.[44] is lower than that of our study, while their MAC_{365} value is higher than that of our study, indicating that the total concentration of atmospheric BrC in 2017 was higher approximately a decade ago. Figure 2c and Figure 2d show that not only are the total chromophore contents in the winter samples higher than those in the other seasons but also the average light absorption capacity and fluorescence ability are higher than those in the other seasons. The high total chromophore contents in the winter samples are related to the higher PM concentration in winter, while the higher light absorption and fluorescence capacities in winter should be determined by the chemical composition and source. For example, the photochemical reaction in winter is relatively weak, which at the same time weakens the bleaching process of chromophore and absorbance.[31,41]

Correlation between the OP and Optical Properties. Previous studies have found that the OP of water-soluble PM has a certain correlation with the WSOC and BrC.[16,22,48,49] This study also yielded similar results. As shown in Table 1, the

Table 1. Correlations between the DTTv Activity and WSOC; Abs_{365}; TFV; EC; $Abs_{365,BrC3}$; C7; and Selected Metal Elements (Cu, Fe, Mn, V, and Zn) (n = 112)

	correlation coefficient (r) and significance level (p, two-sided test)	
constituents	r	p
WSOC	0.85	<0.000
Abs_{365}	0.72	<0.000
TFV	0.59	<0.000
EC	0.64	<0.000
$Abs_{365,BrC3}$	0.73	<0.000
C7	0.65	<0.000
Cu	0.48	<0.000
Fe	0.19	0. 042
Mn	0.38	<0.000
V	0.07	0. 471
Zn	0.46	<0.000

DTT activity of WSM is significantly positively correlated with the WSOC content (r = 0.85, $p < 0.000$), suggesting that the organic matter in water-soluble substances may have an important contribution to the DTT activity. Table 1 also lists the metal elements corresponding to the water-soluble metals associated with DTT consumption reported in several studies.[16,34] However, these metal elements are not strongly correlated with DTT activity. Note that the metal elements here refer to the total metal elements in the PM particles. The

DOI: 10.1021/acs.est.9b01976
Environ. Sci. Technol. XXXX, XXX, XXX−XXX

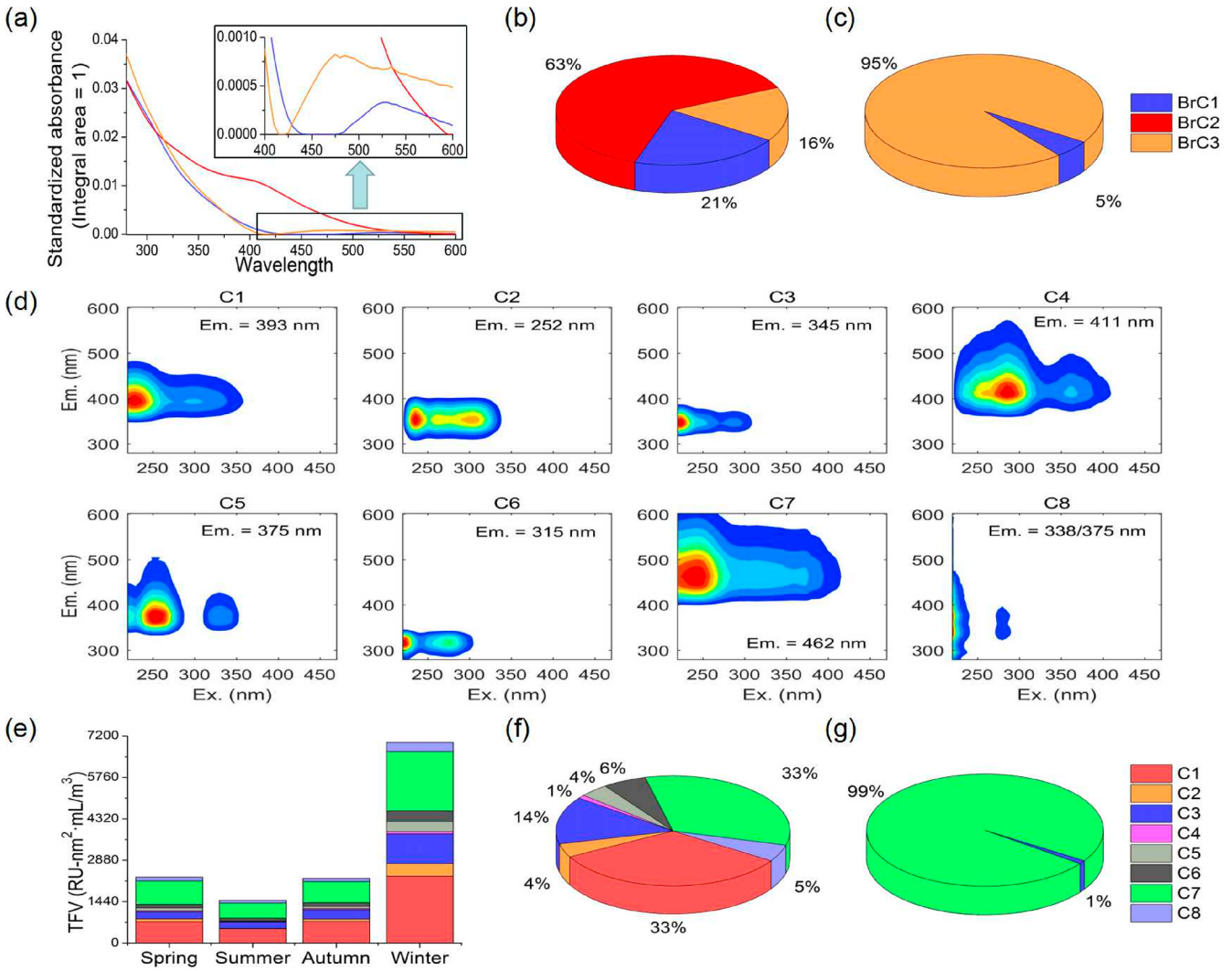

Figure 3. (a) Three-factor BrC optical absorption spectra analyzed by the NMF model. (b) Relative percentage of light absorption of the three types of BrC at 365 nm. (c) Percentage of relative contributions of the three types of BrC to the DTTv activity. (d) EEM profiles of the chromophores derived from the PARAFAC model for the WSOM of the $PM_{2.5}$ samples. (e) TFVs of the different chromophores in the spring, summer, autumn, and winter of 2017. (f) Relative contributions of the different chromophores to the total fluorescent signal. (g) Relative contributions of the different chromophores to the DTTv activity.

correlation between the other metal elements and DTT consumption is also given in Table S5. Previous studies have confirmed that the organic matter can generate ROS in atmospheric particulates, such as quinones,[15] HULIS,[16,17] and polycyclic aromatic hydrocarbons (PAHs).[50] Verma et al.[22] found that the DTT activity in water-soluble PM has a significant positive correlation with BrC but is not correlated with any metals. Organic substances may represent the important causes of DTT consumption and may be mainly contributed by light absorbing materials. Similar to the results of Verma et al.,[22] this study also found a significant correlation (r = 0.72, p < 0.000, Table 1) between the DTT activity and BrC content (both Abs_{365} and Abs_{500}, absorbance at 500 nm), which is consistent with organic substances with light absorbing properties being important contributors to the DTT activity levels of the studied samples. Furthermore, we also explored the relationship between the DTT activity and fluorescence characteristics. EEM spectroscopy can provide more material class information than light absorption spectroscopy, although the EEM-measured chromophores may only represent part of the BrC substances. We found that the DTT activity was also correlated with the FV (r = 0.59, p < 0.000, Table 1), which suggested that the DTT activity is related not only to light absorbing substances but also to fluorescent substances. The light absorbing and fluorescent substances generally have large conjugated electron systems,[51] such as quinones and PAHs, which are currently recognized substances in PM that cause damage to humans.

The DTT activity and EC levels of the whole year samples were significantly positively correlated (r = 0.64, Table 1), suggesting that the combustion source may be an important contributor to the DTT activity in $PM_{2.5}$ over Xi'an. The DTT activity levels in different seasons are also related to WSOC and TFV (Figure S4). The correlation between WSOC and TFV with the DTT activity in autumn is significantly greater than that in the other seasons. The correlation between K^+ and DTT activity in autumn is also greater than that in the other seasons (Table S6), suggesting that biomass burning and mineral dust are the main contributors to the DTT activity in autumn. In addition, the correlation between Ca and DTT is

DOI: 10.1021/acs.est.9b01976
Environ. Sci. Technol. XXXX, XXX, XXX−XXX

also strong (r = 0.54, Table S5), suggesting that a dust source may contribute to the DTT activity.

Structure−Activity Relationship between the Optical Properties and OP. To better explore the structure−activity relationship between the DTT activity and BrC, we used the NMF model to resolve the BrC into three factors, named BrC1, BrC2, and BrC3 (shown in Figure 3a). The spectra of BrC1−3 show that the overall spectra of BrC1 and BrC3 are similar but differ greatly from that of BrC2. The factors all have distinct absorption peaks with peaks at 530, 480, and 400 nm. As shown in Figure 3b, BrC2 contributed 63 ± 7% of the total absorbance at 365 nm, while BrC1 and BrC3 contributed 21 ± 8% and 16 ± 2% of the absorbance, respectively. Moreover, the BrC2 relative light absorption contribution does not change significantly with the season (Figure S5). The relative contribution of BrC2 to light absorption increases with increasing wavelength to 80 ± 3% at 500 nm, whereas the relative contributions of BrC1 and BrC3 are reduced to 5 ± 2% and 15 ± 2%, respectively (Figure S6). The above results indicate that the BrC2 species are major contributors to light absorption in the full wavelength range, while BrC1 and BrC3 are only partial light absorption contributors. Interestingly, the contributions of the BrC factors to the DTT activity are inconsistent with the light absorption contributions. As shown in Figure 3c, in the contribution of total BrC to DTT activity, 95 ± 2% of the DTT activity is contributed by BrC3, and BrC1 only accounted for 5 ± 2%, while BrC2 does not contribute to the DTT activity. The study also found that the absorbance of BrC3 at 365 nm is significantly positively correlated with the DTT activity (r = 0.73, p < 0.000, Table 1), thus suggesting that the contribution of BrC to DTT activity is mainly associated with BrC3. Figure 3a shows that BrC1 and BrC3 have distinct absorption peaks in the long-wavelength range of 480−530 nm, but there is no peak of BrC2. This feature may be related to the contributions of BrC1 and BrC3 to the DTT activity. In general, the fact that a substance has an absorption peak at a long wavelength means that the substance may contain a large delocalized conjugated electron system, such as a quinone n−π* electron, a PAH substance π−π* electron, or the like.[51] These substances having conjugated electrons are more likely to transmit electrons to undergo a catalytic reaction, thereby contributing to DTT activity.

Certain BrC substances can generate fluorescent compounds, such as aromatic hydrocarbons,[52,53] quinones,[54] proteinaceous substances,[55−57] and phenolic substances,[58] which may be important substances for generating DTT activity in colored WSOM. Due to the complexity of the actual atmospheric aerosol, we are unable to fully identify the substance in the actual aerosol, but the chromophore can provide us with more detailed information on the organic matter. To this end, we characterized the fluorescence properties of the samples using the EEM method to explore the intrinsic relationship between the different chromophores and DTT activity levels. The results are shown in Figure 3d. The eight chromophores derived from PARAFAC are designated C1−C8. These chromophores are defined in terms of the excitation and emission wavelengths with reference to previous studies, where C1, C4, C5, and C8 may be certain low-oxidation HULIS,[31,53,59] C2 may be a certain HULIS or proteinaceous material,[56] C3 may be a proteinaceous substance,[55] C6 may be a tyrosine,[60] and C7 may be a highly oxidized HULIS or aromatic hydrocarbon or quinone.[31,53,54] The HULIS chromophore in this study is the primary chromophore type in atmospheric particulates, which is similar to the results of Fu et al.[61] The relative contributions of the different chromophores to the FVs of the four seasons remained essentially unchanged (Figure S7). Only the TFV produced significant seasonal changes (Figure 3e). The FV in winter is significantly higher than those in the other seasons. From the annual average fluorescence contribution (Figure 3f), the HULIS-like chromophores C1 and C7 accounted for the majority of the FV, totaling approximately 70%.

Figure 3g shows the relative contributions of the different chromophores to the DTT activity in the contribution of total chromophore to DTT activity, of which only chromophores C3 and C7 contribute to the DTT activity, almost all of which is attributed to the C7 chromophore (99%), although chromophore C7 accounts for only 33% of the TFV. Chromophore C7 has a remarkable feature compared with other chromophores and has a high emission wavelength of 462 nm. This feature reveals that some fraction of the DTT active material in PM should be a substance containing a large conjugated electron functional group, such as a hydroxy arene, a quinone, or the like having electron donor and acceptor functional groups.[62] This result is similar to the conclusion of the light absorption analysis. In particular, the C7 spectrum is very similar to the EEM spectra of PAHs or quinone compounds,[31,52] which have been identified as PAH-like chromophores. DTT consumption is likely to be mainly produced by compounds similar in structure to PAHs, such as hydroxylated or carbonylated PAHs, graphene oxide, and the like. Studies by Huang et al.[44] have shown that the particles over Xi'an are rich in PAHs and hydroxylated or carbonylated PAHs and significantly positively correlated with the absorbance. Li et al.[6] also reported a significant correlation between the DTT activity and PAH content (r^2 = 0.98). These materials with conjugated electrons generally have higher redox potential substitution groups.[63] These groups contain delocalized π electrons, which are more likely to efficiently transfer electrons and form a reversible redox reaction system.[15] At the same time, electron migration (such as the charge transfer between hydrazine and hydroxyl aromatics) occurs between different functional groups intermolecularly or intramolecularly[51] and may also contribute to the DTT oxidation activity of PM.

The correlation analysis between the C1−C8 chromophores and DTT activity levels is shown in Table S7. The results show that there is a positive correlation between the C1−C8 chromophores and DTT activity levels, but the correlation between the C7 chromophore and DTT activity is the most significant (r = 0.65, p < 0.000, Table 1). The correlations between the C7 chromophore and DTT activity in autumn and winter are higher than those in spring and summer (Figure S8), which may be related to increased biomass burning and mineral dust in autumn. Because the K^+ concentration in autumn is second only to that in winter (Table S1−S4), the correlation of the K^+ concentration with the DTT activity and C7 FV in autumn is the strongest (r = 0.88 and 0.83, respectively; Table S6). However, due to the lower overall PM concentration in autumn, the overall DTT activity levels of the autumn samples are lower than those of the other seasons. In winter, not only is the total DTT activity high but the correlation between the C7 chromophore and DTT activity is also high. This aspect may be due to the large amounts of PAH-like and quinone-like compounds with high DTT activity levels being emitted into the atmosphere due to the burning of

DOI: 10.1021/acs.est.9b01976
Environ. Sci. Technol. XXXX, XXX, XXX−XXX

large amounts of fossil fuels.[16,64] On the other hand, weaker light causes the bleaching reaction in winter to be weaker than in other seasons, reducing the loss of BrC and chromophores.[31]

As discussed above, both the absorbance and fluorescence factor analyses indicated that PAH-like or quinone-like chromophoric substances may be important substances in the light absorbing water-soluble PM that contribute to the DTT oxidation activity. These substances are mainly substances with aromatic hydrocarbons and quinone structures and not only PAHs and quinone. However, in this study, the amount of DTT oxidation activity contributed by these chromophores and how much the total DTT oxidation activity is caused by organic matter remain unclear. Xiong et al.[65] found that the ROS produced by metal ions, such as Cu (II) and Fe (II, III), was not significant. However, Yu et al.[66] found that Fe and quinones have synergistic effects and can produce · OH by the Fenton reaction, which further indicates that organic matter is an important substance in PM that can induce ROS. The contributions of organic and inorganic substances to DTT activity cannot be considered separately since at least part of the DTT activity may be due to their synergistic mechanism. Nonetheless, this study demonstrates that organic matter contributes significantly to DTT activity, and only a small fraction and a particular class of chromophore species contribute to the vast majority of DTT activity in light absorbing organics. This discovery will help to better interpret and understand the mechanism of oxidation activity generation by light absorbing organic aerosols and provide insights for predicting the OP of light absorbing organic aerosols based on their optical properties. In addition, the oxidative active substances in colored WSOM that we have identified that mainly consume DTT are based on the optical properties, that is, a cluster of compounds with similar light absorption and fluorescence properties. The substance or chemical structure of such a chromophore substance has not been clarified, and such information will depend on future research progress on the chemical characteristics of BrC aerosols.

■ ENVIRONMENTAL IMPLICATIONS

OP is an important inducement and evaluation index of the currently accepted harm to human health caused by aerosols. Research on the relationship between the aerosol chemical composition and OP is the hottest and most challenging scientific issue. Certain studies have revealed that metal elements contribute significantly to the OP of atmospheric PM.[34,67] However, other studies have shown that organic components may be important contributors to the OP rather than transition metals,[65,68] which should be determined by the aerosol chemical composition and source.[68] The results of this study show that BrC species in the organic components may be important contributors to the OP of the PM over Xi'an. This conclusion was supported by earlier research by Verma et al.[22] Based on this result, this study has further studied the chromophores that contribute to the OP of light absorbing water-soluble PM. We divided the components of PM into material classes with different optical properties through factor analysis techniques. Only a small part of the special chromophores (BrC3 and C7) contributed most to the DTT activity of colored WSOM in PM. These chromophores each had a long absorption wavelength and a fluorescence emission wavelength, and these characteristics revealed that these chromophores should be those containing larger conjugated electrons. This new knowledge will help to better interpret and understand the mechanism of oxidation activity generation by light absorbing organic aerosols.

At present, the organic substances that produce OP in water-soluble PM are mainly quinones, HULIS, and the like.[15,16] However, the compositions of these substances in PM are complex and variable. Certain studies attempt to simulate the production of OP through certain typical compounds, but this approach only explains the partial OP level.[34,65] For example, Jin et al.[68] showed that PAHs and metals contribute less than 50% to $PM_{2.5}$-induced ROS. We know that organic aerosol components are very complex. At present, analytical techniques are not able to achieve complete qualitative and quantitative analyses, and the OP levels of different substances are very different; therefore, it is difficult or even impossible to explain the overall OP of PM at a specific single molecular level. From the perspective of the optical characteristics of the complex aerosol components, this study screened clusters of compounds that have important contributions to the DTT oxidation activity levels of colored organic aerosols rather than a specific molecule or molecules. This holistic approach based on the aerosol optical properties provides a new method of studying the aerosol OP, such as by using a quantitative relationship between the optical absorption properties and the OP of aerosols to predict and evaluate global simulations of human health damage based on BrC.[69,70]

This study has obtained the important result that BrC3 and C7 are important contributors to the DTT activity of colored water-soluble PM. However, the chromophore materials and chemical structures as well as their sources and formation mechanisms have not been clarified. These findings require further research in the future to deepen the understanding of the mechanism and source of PM OP.

■ ASSOCIATED CONTENT

Supporting Information

The Supporting Information is available free of charge on the ACS Publications website at DOI: 10.1021/acs.est.9b01976.

Tables S1−S7; Figures S1−S11; EC analysis; water-soluble ion analysis and elemental analysis (PDF)

■ AUTHOR INFORMATION

Corresponding Author

*E-mail: chenqingcai@sust.edu.cn. Phone/fax: (+86) 029-86132765.

ORCID

Qingcai Chen: 0000-0001-7450-0073

Notes

The authors declare no competing financial interest.

■ ACKNOWLEDGMENTS

This work was supported by the National Natural Science Foundation of China (grant numbers: 41877354 and 41703102) and the Nature Science Foundation of Shaanxi Province, China (2018JM4011).

■ REFERENCES

(1) Hoek, G.; Brunekreef, B.; Goldbohm, S.; Fischer, P.; van den Brandt, P. A. Association between mortality and indicators of traffic-related air pollution in the Netherlands: a cohort study. *Lancet* **2002**, *360* (9341), 1203−1209.

DOI: 10.1021/acs.est.9b01976
Environ. Sci. Technol. XXXX, XXX, XXX−XXX

(2) Riediker, M.; Cascio, W. E.; Griggs, T. R.; Herbst, M. C.; Bromberg, P. A.; Neas, L.; Williams, R. W.; Devlin, R. B. Particulate matter exposure in cars is associated with cardiovascular effects in healthy young men. *Am. J. Respir. Crit. Care Med.* **2004**, *169* (8), 934−940.
(3) Peel, J. L.; Tolbert, P. E.; Klein, M.; Metzger, K. B.; Flanders, W. D.; Todd, K.; Mulholland, J. A.; Ryan, P. B.; Frumkin, H. Ambient air pollution and respiratory emergency department visits. *Epidemiology* **2005**, *16* (2), 164−174.
(4) Ayres, J. G.; Borm, P.; Cassee, F. R.; Castranova, V.; Donaldson, K.; Ghio, A.; Harrison, R. M.; Hider, R.; Kelly, F.; Kooter, I. M.; et al. Evaluating the toxicity of airborne particulate matter and nanoparticles by measuring oxidative stress potential—a workshop report and consensus statement. *Inhal. Toxicol.* **2008**, *20* (1), 75−99.
(5) Solomon, P. A.; Costantini, M.; Grahame, T. J.; Gerlofs-Nijland, M. E.; Cassee, F. R.; Russell, A. G.; Brook, J. R.; Hopke, P. K.; Hidy, G.; Phalen, R. F.; et al. Air pollution and health: bridging the gap from sources to health outcomes: conference summary. *Air Qual. Atmos. Hlth.* **2012**, *5* (1), 9−62.
(6) Li, N.; Sioutas, C.; Cho, A.; Schmitz, D.; Misra, C.; Sempf, J.; Wang, M. Y.; Oberley, T.; Froines, J.; Nel, A. Ultrafine particulate pollutants induce oxidative stress and mitochondrial damage. *Environ. Health Perspect.* **2003**, *111* (4), 455−460.
(7) Squadrito, G. L.; Cueto, R.; Dellinger, B.; Pryor, W. A. Quinoid redox cycling as a mechanism for sustained free radical generation by inhaled airborne particulate matter. *Free Radical Biol. Med.* **2001**, *31* (9), 1132−1138.
(8) Kelly, F. J.; Fussell, J. C. Size, source and chemical composition as determinants of toxicity attributable to ambient particulate matter. *Atmos. Environ.* **2012**, *60*, 504−526.
(9) Li, N.; Wang, M. Y.; Bramble, L. A.; Schmitz, D. A.; Schauer, J. J.; Sioutas, C.; Harkema, J. R.; Nel, A. E. The Adjuvant Effect of Ambient Particulate Matter Is Closely Reflected by the Particulate Oxidant Potential. *Environ. Health Perspect.* **2009**, *117* (7), 1116−1123.
(10) Donaldson, K.; Brown, D.; Clouter, A.; Duffin, R.; MacNee, W.; Renwick, L.; Tran, L.; Stone, V. The pulmonary toxicology of ultrafine particles. *J. Aerosol Med.* **2002**, *15* (2), 213−220.
(11) Nel, A. Air pollution-related illness: effects of particles. *Science* **2005**, *308* (5723), 804−806.
(12) Pope, C. A.; Dockery, D. W. Health effects of fine particulate air pollution: Lines that connect. *J. Air Waste Manage. Assoc.* **2006**, *56* (6), 709−742.
(13) Cho, A. K.; Sioutas, C.; Miguel, A. H.; Kumagai, Y.; Schmitz, D. A.; Singh, M.; Eiguren-Fernandez, A.; Froines, J. R. Redox activity of airborne particulate matter at different sites in the Los Angeles Basin. *Environ. Res.* **2005**, *99* (1), 40−47.
(14) Brook, R. D.; Rajagopalan, S.; Pope, C. A., III; Brook, J. R.; Bhatnagar, A.; Diez-Roux, A. V.; Holguin, F.; Hong, Y.; Luepker, R. V.; Mittleman, M. A.; Peters, A.; Siscovick, D.; Smith, S. C., Jr; Whitsel, L.; Kaufman, J. D. Particulate matter air pollution and cardiovascular disease: An update to the scientific statement from the American Heart Association. *Circulation* **2010**, *121*, 2331−2378.
(15) Kumagai, Y.; Koide, S.; Taguchi, K.; Endo, A.; Nakai, Y.; Yoshikawa, T.; Shimojo, N. Oxidation of proximal protein sulfhydryls by phenanthraquinone, a component of diesel exhaust particles. *Chem. Res. Toxicol.* **2002**, *15* (4), 483−489.
(16) Lin, P.; Yu, J. Z. Generation of Reactive Oxygen Species Mediated by Humic-like Substances in Atmospheric Aerosols. *Environ. Sci. Technol.* **2011**, *45* (24), 10362−10368.
(17) Verma, V.; Wang, Y.; El-Afifi, R.; Fang, T.; Rowland, J.; Russell, A. G.; Weber, R. J. Fractionating ambient humic-like substances (HULIS) for their reactive oxygen species activity − Assessing the importance of quinones and atmospheric aging. *Atmos. Environ.* **2015**, *120*, 351−359.
(18) Fang, T.; Verma, V.; Bates, J. T.; Abrams, J.; Klein, M.; Strickland, M. J.; Sarnat, S. E.; Chang, H. H.; Mulholland, J. A.; Tolbert, P. E.; Russell, A. G.; Weber, R. J. Oxidative potential of ambient water-soluble PM2.5 in the southeastern United States: contrasts in sources and health associations between ascorbic acid (AA) and dithiothreitol (DTT) assays. *Atmos. Chem. Phys.* **2016**, *16* (6), 3865−3879.
(19) Charrier, J. G.; Anastasio, C. Impacts of antioxidants on hydroxyl radical production from individual and mixed transition metals in a surrogate lung fluid. *Atmos. Environ.* **2011**, *45* (40), 7555−7562.
(20) Verma, V.; Fang, T.; Xu, L.; Peltier, R. E.; Russell, A. G.; Ng, N. L.; Weber, R. J. Organic aerosols associated with the generation of reactive oxygen species (ROS) by water-soluble $PM_{2.5}$. *Environ. Sci. Technol.* **2015**, *49*, 4646−4656.
(21) Charrier, J. G.; Anastasio, C. On dithiothreitol (DTT) as a measure of oxidative potential for ambient particles: evidence for the importance of soluble transition metals. *Atmos. Chem. Phys.* **2012**, *12* (19), 9321−9333.
(22) Verma, V.; Rico-Martinez, R.; Kotra, N.; King, L.; Liu, J. M.; Snell, T. W.; Weber, R. J. Contribution of Water-Soluble and Insoluble Components and Their Hydrophobic/Hydrophilic Subfractions to the Reactive Oxygen Species-Generating Potential of Fine Ambient Aerosols. *Environ. Sci. Technol.* **2012**, *46* (20), 11384−11392.
(23) Chen, Q.; Sun, H.; Wang, M.; Mu, Z.; Wang, Y.; Li, Y.; Wang, Y.; Zhang, L.; Zhang, Z. Dominant Fraction of EPFRs from Nonsolvent-Extractable Organic Matter in Fine Particulates over Xi'an, China. *Environ. Sci. Technol.* **2018**, *52*, 9646−9655.
(24) Lawaetz, A. J.; Stedmon, C. A. Fluorescence Intensity Calibration Using the Raman Scatter Peak of Water. *Appl. Spectrosc.* **2009**, *63* (8), 936−940.
(25) Murphy, K. R.; Butler, K. D.; Spencer, R. G. M.; Stedmon, C. A.; Boehme, J. R.; Aiken, G. R. Measurement of Dissolved Organic Matter Fluorescence in Aquatic Environments: An Interlaboratory Comparison. *Environ. Sci. Technol.* **2010**, *44* (24), 9405−9412.
(26) Arangio, A. M.; Tong, H.; Socorro, J.; Pöschl, U.; Shiraiwa, M. Quantification of environmentally persistent free radicals and reactive oxygen species in atmospheric aerosol particles. *Atmos. Chem. Phys.* **2016**, *16* (20), 13105−13119.
(27) Liu, W.; Xu, Y.; Liu, W.; Liu, Q.; Yu, S.; Liu, Y.; Wang, X.; Tao, S. Oxidative potential of ambient PM2.5 in the coastal cities of the Bohai Sea, northern China: Seasonal variation and source apportionment. *Environ. Pollut.* **2018**, *236*, 514−528.
(28) Bates, J. T.; Weber, R. J.; Abrams, J.; Verma, V.; Fang, T.; Klein, M.; Strickland, M. J.; Sarnat, S. E.; Chang, H. H.; Mulholland, J. A.; Tolbert, P. E.; Russell, A. G. Reactive oxygen species generation linked to sources of atmospheric particulate matter and cardiorespiratory effects. *Environ. Sci. Technol.* **2015**, *49* (22), 13605−13612.
(29) Pauca, V. P.; Piper, J.; Plemmons, R. J. Nonnegative matrix factorization for spectral data analysis. *Linear Algebra Appl.* **2006**, *416* (1), 29−47.
(30) Murphy, K. R.; Stedmon, C. A.; Graeber, D.; Bro, R. Fluorescence spectroscopy and multi-way techniques. *Anal. Methods* **2013**, *5*, 6557−6566.
(31) Chen, Q.; Miyazaki, Y.; Kawamura, K.; Matsumoto, K.; Coburn, S.; Volkamer, R.; Iwamoto, Y.; Kagami, S.; Deng, Y.; Ogawa, S. Characterization of Chromophoric Water-Soluble Organic Matter in Urban, Forest, and Marine Aerosols by HR-ToF-AMS Analysis and Excitation−Emission Matrix Spectroscopy. *Environ. Sci. Technol.* **2016**, *50* (19), 10351−10360.
(32) Li, Y.; Ngom, A. The non-negative matrix factorization toolbox for biological data mining. *Source Code Biol. Med.* **2013**, *8* (1), 1−15.
(33) Liu, Q. Y.; Baumgartner, J.; Zhang, Y. X.; Liu, Y. J.; Sun, Y. J.; Zhang, M. G. Oxidative Potential and Inflammatory Impacts of Source Apportioned Ambient Air Pollution in Beijing. *Environ. Sci. Technol.* **2014**, *48* (21), 12920−12929.
(34) Lyu, Y.; Guo, H.; Cheng, T.; Li, X. Particle Size Distributions of Oxidative Potential of Lung-Deposited Particles: Assessing Contributions from Quinones and Water-Soluble Metals. *Environ. Sci. Technol.* **2018**, *52* (11), 6592−6600.
(35) Chirizzi, D.; Cesari, D.; Guascito, M. R.; Dinoi, A.; Giotta, L.; Donateo, A.; Contini, D. Influence of Saharan dust outbreaks and

DOI: 10.1021/acs.est.9b01976
Environ. Sci. Technol. XXXX, XXX, XXX−XXX

carbon content on oxidative potential of water-soluble fractions of $PM_{2.5}$ and PM_{10}. *Atmos. Environ.* **2017**, *163*, 1−8.
(36) Wang, J.; Lin, X.; Lu, L.; Wu, Y.; Zhang, H.; Lv, Q.; Liu, W.; Zhang, Y.; Zhuang, S. Temporal variation of oxidative potential of water soluble components of ambient $PM_{2.5}$ measured by dithiothreitol (DTT) assay. *Sci. Total Environ.* **2019**, *649*, 969−978.
(37) Patel, A.; Rastogi, N. Oxidative potential of ambient fine aerosol over a semi-urban site in the Indo-Gangetic Plain. *Atmos. Environ.* **2018**, *175*, 127−134.
(38) Pietrogrande, M. C.; Dalpiaz, C.; Dell'Anna, R.; Lazzeri, P.; Manarini, F.; Visentin, M.; Tonidandel, G. Chemical composition and oxidative potential of atmospheric coarse particles at an industrial and urban background site in the alpine region of northern italy. *Atmos. Environ.* **2018**, *191*, 340−350.
(39) Janssen, N. A. H.; Yang, A. L.; Strak, M.; Steenhof, M.; Hellack, B.; Gerlofs-Nijland, M. E.; Kuhlbusch, T.; Kelly, F.; Harrison, R. M.; Brunekreef, B.; Hoek, G.; Cassee, F. Oxidative potential of particulate matter collected at sites with different source characteristics. *Sci. Total Environ.* **2014**, *472*, 572−581.
(40) Tong, H. J.; Lakey, P. S. J.; Arangio, A. M.; Socorro, J.; Shen, F. X.; Lucas, K.; Brune, W. H.; Poschl, U.; Shiraiwa, M. Reactive Oxygen Species Formed by Secondary Organic Aerosols in Water and Surrogate Lung Fluid. *Environ. Sci. Technol.* **2018**, *52* (20), 11642−11651.
(41) Chen, Q.; Ikemori, F.; Mochida, M. Light Absorption and Excitation−Emission Fluorescence of Urban Organic Aerosol Components and Their Relationship to Chemical Structure. *Environ. Sci. Technol.* **2016**, *50* (20), 10859−10868.
(42) Zhang, X. L.; Lin, Y. H.; Surratt, J. D.; Weber, R. J. Sources, Composition and Absorption Angstrom Exponent of Light-absorbing Organic Components in Aerosol Extracts from the Los Angeles Basin. *Environ. Sci. Technol.* **2013**, *47* (8), 3685−3693.
(43) Yan, C. Q.; Zheng, M.; Sullivan, A. P.; Bosch, C.; Desyaterik, Y.; Andersson, A.; Li, X. Y.; Guo, X. S.; Zhou, T.; Gustafsson, O.; Collett, J. L. Chemical characteristics and light-absorbing property of water-soluble organic carbon in Beijing: Biomass burning contributions. *Atmos. Environ.* **2015**, *121*, 4−12.
(44) Huang, R.; Yang, L.; Cao, J.; Chen, Y.; Chen, Q.; Li, Y.; Duan, J.; Zhu, C.; Dai, W.; Wang, K.; Lin, C.; Ni, H.; Corbin, J.; Wu, Y.; Zhang, R.; Tie, X.; Hoffmann, T.; O'Dowd, C.; Dusek, U. Brown Carbon Aerosol in Urban Xi'an, Northwest China: The Composition and Light Absorption Properties. *Environ. Sci. Technol.* **2018**, *52* (12), 6825−6833.
(45) Zhang, X.; Lin, Y. H.; Surratt, J. D.; Zotter, P.; Prévôt, A. H. S.; Weber, R. J. Light-absorbing soluble organic aerosol in Los Angeles and Atlanta: A contrast in secondary organic aerosol. *Geophys. Res. Lett.* **2011**, *38*, DOI: 10.1029/2011GL049385.
(46) Cheng, Y.; He, K. B.; Zheng, M.; Duan, F. K.; Du, Z. Y.; Ma, Y. L.; Tan, J. H.; Yang, F. M.; Liu, J. M.; Zhang, X. L.; Weber, R. J.; Bergin, M. H.; Russell, A. G. Mass absorption efficiency of elemental carbon and water-soluble organic carbon in Beijing, China. *Atmos. Chem. Phys.* **2011**, *11* (22), 11497−11510.
(47) Kirillova, E. N.; Andersson, A.; Han, J.; Lee, M.; Gustafsson, O. Sources and light absorption of water-soluble organic carbon aerosols in the outflow from northern China. *Atmos. Chem. Phys.* **2014**, *14* (3), 1413−1422.
(48) Hu, S.; Polidori, A.; Arhami, M.; Shafer, M.; Schauer, J.; Cho, A.; Sioutas, C. Redox activity and chemical speciation of size fractioned PM in the communities of the Los Angeles-Long Beach harbor. *Atmos. Chem. Phys.* **2008**, *8* (21), 6439−6451.
(49) Verma, V.; Polidori, A.; Schauer, J. J.; Shafer, M. M.; Cassee, F. R.; Sioutas, C. Physicochemical and toxicological profiles of particulate matter in Los Angeles during the October 2007 southern California wildfires. *Environ. Sci. Technol.* **2009**, *43* (3), 954−960.
(50) Alam, M. S.; Stark, C.; Delgado-Saborit, J. M.; Harrison, R. M. Using atmospheric measurements of PAH and quinone compounds at roadside and urban background sites to assess sources and reactivity. *Atmos. Environ.* **2013**, *77* (3), 24−35.
(51) Cory, R. M.; McKnight, D. M. Fluorescence spectroscopy reveals ubiquitous presence of oxidized and reduced quinones in dissolved organic matter. *Environ. Sci. Technol.* **2005**, *39* (21), 8142−8149.
(52) Nahorniak, M. L.; Booksh, K. S. Excitation-emission matrix fluorescence spectroscopy in conjunction with multiway analysis for pah detection in complex matrices. *Analyst* **2006**, *131* (12), 1308−1315.
(53) Aryal, R.; Lee, B. K.; Beecham, S.; Kandasamy, J.; Aryal, N.; Parajuli, K. Characterisation of Road Dust Organic Matter as a Function of Particle Size: A PARAFAC Approach. *Water, Air, Soil Pollut.* **2015**, *226*, 1−24.
(54) Mladenov, N.; Alados-Arboledas, L.; Olmo, F. J.; Lyamani, H.; Delgado, A.; Molina, A.; Reche, I. Applications of optical spectroscopy and stable isotope analyses to organic aerosol source discrimination in an urban area. *Atmos. Environ.* **2011**, *45* (11), 1960−1969.
(55) Matos, J. T. V.; Freire, S. M. S. C.; Duarte, R. M. B. O.; Duarte, A. C. Natural organic matter in urban aerosols: Comparison between water and alkaline soluble components using excitation-emission matrix fluorescence spectroscopy and multiway data analysis. *Atmos. Environ.* **2015**, *102*, 1−10.
(56) Salve, P. R.; Lohkare, H.; Gobre, T.; Bodhe, G.; Krupadam, R. J.; Ramteke, D. S.; Wate, S. R. Characterization of Chromophoric Dissolved Organic Matter (CDOM) in Rainwater Using Fluorescence Spectrophotometry. *Bull. Environ. Contam. Toxicol.* **2012**, *88*, 215−218.
(57) Birdwell, J. E.; Valsaraj, K. T. Characterization of dissolved organic matter in fogwater by excitation−emission matrix fluorescence spectroscopy. *Atmos. Environ.* **2010**, *44* (27), 3246−3253.
(58) De Laurentiis, E.; Sur, B.; Maurino, V.; Minero, C.; Mailhot, G.; Brigante, M.; Vione, D.; Pazzi, M. Phenol transformation and dimerisation, photosensitised by the triplet state of 1-nitronaphthalene: A possible pathway to humic-like substances (HULIS) in atmospheric waters. *Atmos. Environ.* **2013**, *70*, 318−327.
(59) Qin, J.; Zhang, L.; Zhou, X.; Duan, J.; Mu, S.; Xiao, K.; Hu, J.; Tan, J. Fluorescence fingerprinting properties for exploring water-soluble organic compounds in $PM_{2.5}$ in an industrial city of northwest China. *Atmos. Environ.* **2018**, *184*, 203−211.
(60) Yu, H.; Liang, H.; Qu, F.; Han, Z. H.; Shao, S.; Chang, H.; Li, G. Impact of dataset diversity on accuracy and sensitivity of parallel factor analysis model of dissolved organic matter fluorescence excitation-emission matrix. *Sci. Rep.* **2015**, *5*, 10207.
(61) Fu, P.; Kawamura, K.; Chen, J.; Qin, M.; Ren, L.; Sun, Y.; Wang, Z.; Barrie, A. L.; Tachibana, E.; Ding, A.; Yamashita, A. Fluorescent water-soluble organic aerosols in the high arctic atmosphere. *Sci. Rep.* **2015**, *5* (5), 9845.
(62) Del Vecchio, R.; Blough, N. V. On the origin of the optical properties of humic substances. *Environ. Sci. Technol.* **2004**, *38* (14), 3885−3891.
(63) Schoonen, M. A. A.; Cohn, C. A.; Roemer, E.; Laffers, R.; Simon, S. R.; O'Riordan, T. Mineral-induced formation of reactive oxygen species. *Rev. Mineral. Geochem.* **2006**, *64* (1), 179−221.
(64) Genualdi, S. A.; Killin, R. K.; Woods, J.; Wilson, G.; Schmedding, D.; Simonich, S. L. M. Trans-Pacific and Regional Atmospheric Transport of Polycyclic Aromatic Hydrocarbons and Pesticides in Biomass Burning Emissions to Western North America. *Environ. Sci. Technol.* **2009**, *43* (4), 1061−1066.
(65) Xiong, Q.; Yu, H.; Wang, R.; Wei, J.; Verma, V. Rethinking Dithiothreitol-Based Particulate Matter Oxidative Potential: Measuring Dithiothreitol Consumption versus Reactive Oxygen Species Generation. *Environ. Sci. Technol.* **2017**, *51*, 6507−6514.
(66) Yu, H.; Wei, J.; Cheng, Y.; Subedi, K.; Verma, V. Synergistic and antagonistic interactions among the particulate matter components in generating reactive oxygen species based on the dithiothreitol assay. *Environ. Sci. Technol.* **2018**, *52* (4), 2261−2270.
(67) See, S. W.; Wang, Y. H.; Balasubramanian, R. Contrasting reactive oxygen species and transition metal concentrations in combustion aerosols. *Environ. Res.* **2007**, *103* (3), 317−324.

DOI: 10.1021/acs.est.9b01976
Environ. Sci. Technol. XXXX, XXX, XXX−XXX

(68) Jin, L.; Xie, J.; Wong, C. K.; Chan, Y. K.; Abbaszade, G.; Schnelle-Kreis, J.; Zimmermann, R.; Li, J.; Zhang, G.; Fu, p.; Li, X. Contributions of City-Specific Fine Particulate Matter ($PM_{2.5}$) to Differential In Vitro Oxidative Stress and Toxicity Implications between Beijing and Guangzhou of China. *Environ. Sci. Technol.* **2019**, *53* (5), 2881−2891.
(69) Wang, X.; Heald, C. L.; Liu, J.; Weber, R. J.; Campuzano-Jost, P.; Jimenez, J. L.; Schwarz, J. P.; Perring, A. E. Exploring the observational constraints on the simulation of brown carbon. *Atmos. Chem. Phys.* **2018**, *18* (2), 635−653.
(70) Hammer, M. S.; Martin, R. V.; van Donkelaar, A.; Buchard, V.; Torres, O.; Ridley, D. A.; Spurr, R. J. D. Interpreting the Ultraviolet Aerosol Index observed with the OMI satellite instrument to understand absorption by organic aerosols: implications for atmospheric oxidation and direct radiative effects. *Atmos. Chem. Phys.* **2016**, *16* (4), 2507−2523.

DOI: 10.1021/acs.est.9b01976
Environ. Sci. Technol. XXXX, XXX, XXX−XXX